https://doi.org/10.3311/PPci.22258
Creative Commons Attribution

Periodica Polytechnica Civil Engineering, 67(4), pp. 1273–1283, 2023

Overconsolidated Stress and Strain Condition of Pavement Layers as a Result of Preloading during Construction

Máté János Vámos[1,2*], János Szendefy[1]

[1] Department of Engineering Geology and Geotechnics, Faculty of Civil Engineering, Budapest University of Technology and Economics, Műegyetem rkp. 3, H-1111 Budapest, Hungary
[2] CDM Smith Consult GmbH, Darmstädter Str. 63, 64404 Bickenbach, Germany
* Corresponding author, e-mail: mate.vamos@cdmsmith.com

Received: 24 March 2023, Accepted: 17 July 2023, Published online: 27 July 2023

Abstract

The stiffness and resilient behavior of soils are essential input properties when designing pavements. There are many material models that take into account the stress dependency of stiffness. In pavements, horizontal stresses generally differ from conventional soils because of the preloading of the pavement during construction. In this research, standardized pavement cross sections were analyzed using finite element software with advanced soil constitutive models, and equations describing their behavior were calibrated with the back-analysis of in-situ and laboratory measurements. The pavement was modelled as comprising 4 layers: asphalt pavement, well graded crushed stone base course, granular subbase course and fine-medium sandy subgrade. The ratio of horizontal and vertical stresses σ_3/σ_1 and strains $\varepsilon_3/\varepsilon_1$ were investigated and assessed in the function of depth and loading, and recommendations are given for the description of these functions. The recommendations give useful input data for future practical applications such as simplified calculation methods that are capable of determining the permanent settlement beneath flexible pavements without the use of finite element methods.

Keywords

pavements, overconsolidation, earth pressure coefficient, horizontal and vertical strain ratio

1 Introduction

One of the most important inputs when designing pavements is the resilient stiffness of the subgrade, the granular subbase and the unbound granular (crushed stone aggregate) base course as these parameters are needed to determine the stresses developing in the asphalt course under axle loads. Either a traditional [1–3] or an analytical [4–6] design procedure is used, the resilient behavior of the soil is highly idealized and it is considered with linearly or non-linearly elastic material models. Stiffness of the soil is often characterized by a value obtained from static measurements such as on-site plate load test (E_2) or CBR test. In a more sophisticated approach, the resilient modulus (M_R) is used, which can be determined by cyclic triaxial testing. These linearly or non-linearly elastic (E–ν and k–Θ) material models highly idealize the complex behavior of the soil. Stiffness of the soil is the function of mean effective normal stress, relative density and strain level and these parameters are not constant either with depth or loading process.

The influence of mean effective normal stress on the stiffness of granular soils is considerable and the stiffness increases with increasing stress. The relationship according to [7] is shown in Eq. (1).

$$G_{max} = A_G \frac{(a_G - e)^2}{1+e} \left(\frac{p}{p_{atm}} \right)^{n_G} p_{atm}, \tag{1}$$

where:

G_{max} is the small strain shear modulus,
e is the void ratio,
p is the mean effective normal stress,
p_{atm} is the atmospheric pressure,
A_G, a_G and n_G are material constants.

With increasing normal stress, the soil particles are pressed together more, so a stiffer behavior is experienced and the value of G_{max} increases. In addition, increasing effective normal stress has favorable effect on the degradation curve also [8], as it increases the linear threshold

Cite this article as: Vámos, M. J., Szendefy, J. "Overconsolidated Stress and Strain Condition of Pavement Layers as a Result of Preloading during Construction", Periodica Polytechnica Civil Engineering, 67(4), pp. 1273–1283, 2023. https://doi.org/10.3311/PPci.22258

shear strain so the small strain stiffness will be valid in a larger strain range. For unbound granular base and subbase materials, the resilient modulus M_R can be calculated using the relationship shown in Eq. (2) [3].

$$M_R = k_1 \theta^{k_2}, \tag{2}$$

where:

Θ is the bulk stress,

k_1 and k_2 are material constants.

As Eqs. (1) and (2) show, the stiffness is determined either by p mean effective normal stress or Θ bulk stress, the principal stresses are needed, and these stresses will be the vertical and horizontal stresses in the axis of the wheel. It was highlighted in [9] that the vertical and horizontal stresses, and thus the stiffness, are constantly changing throughout the entire loading process. Determining the vertical stress is generally not a problem, as it is easy to calculate it from the stress distribution of the wheel load, e.g., using Bussinesq theory. However, several difficulties arise when the horizontal stresses are to be determined. In triaxial testing, the minor principal stress is generally constant and equal to the cell pressure. However, the stresses in field produced by the passage of a wheel consists of repeated vertical and horizontal stresses and repeated reversing shear stresses [9]. Accordingly, the strain trajectories are multidimensional in a pavement beneath a rolling wheel load, i.e., the principal stresses are rotating during loading [10].

As mentioned, determination of the vertical stress from wheel load is trivial when assuming elastic behavior. However, the horizontal stress produced by a rolling wheel requires more analysis in preloaded and overconsolidated pavements. Another rarely analyzed effect in pavements is the deformation and stress state in the soil beneath the asphalt in response to a wheel load. Traditional settlement calculations assume that the load generates one-dimensional compression in the soil, i.e., the strain in horizontal direction is zero. Laterally confined soils behave stiffer than unconfined soils, thus settlements and deformations will be smaller. However, if lateral deformation is allowed, e.g., in a triaxial cell, the soil will behave softer leading to larger deformations and settlements.

There is no consensus in the literature regarding the relationship between vertical and horizontal stresses and strains under a wheel load when preloading and overconsolidation of the soil are also considered. To analyze this relationship, finite element calculations were performed on standardized pavement cross-sections by considering the effect of preloading due to construction traffic and compaction. The goal of these calculations was to analyze the vertical and horizontal stresses and strains, their ratio in the axis of the wheel, and their variation with the magnitude of wheel load; in other words what is the coefficient of earth pressure with depth $K_{xy}(z)$ and the ratio of horizontal and vertical strains $\vartheta(z) = \varepsilon_x/\varepsilon_z$.

The ultimate goal of this research was to develop such a simplified calculation method in analogy with the laminar models of [11–13] that is capable of determining the permanent settlement beneath flexible pavements without the use of finite element methods.

2 Structure of the analyzed pavements

In this research, the standardized pavement cross-sections of the Hungarian Highway Specifications [1] were used. The main characteristics of the standardized pavement sections are presented in Table 1.

The pavement was modelled as comprising 4 layers (sandy subgrade, granular subbase course, well graded crushed stone base course and asphalt pavement). The subgrade was assumed to be a fine-medium sand (denoted as L26 in [14]). This is overlain by subbase course of 20 cm thickness providing a sufficient bearing capacity. This course comprises a 50–50% mixture of 0–11 mm sandy gravel from Tiszatarján and 0–22 mm crushed stone from Gyöngyössolymos (the mixture is described in detail in [15]). On top of the subbase course, unbound granular base course of 20 cm thickness is placed comprising well graded crushed stone aggregate as it is shown in Table 1; this material is described in detail in the works of [16] and [17]. Particle size distribution of the pavement layers is shown in Fig. 1, whereas their properties are summarized in Table 2. The asphalt course was considered as a homogeneous layer, which can be characterized by its traffic load class-dependent thickness, Young's modulus and Poisson's ratio.

Table 1 Standardized pavement cross-sections according to [1]

Traffic load class	Design traffic (million axles)	Thickness of Base course (cm)	Thickness of AC-layer (cm)
A	0.03–0.1	20	10
B	0.1–0.3	20	12
C	0.3–1.0	20	15
D	1.0–3.0	20	18
E	3.0–10.0	20	22
K	10.0–30.0	20	25
R	Over 30	20	29

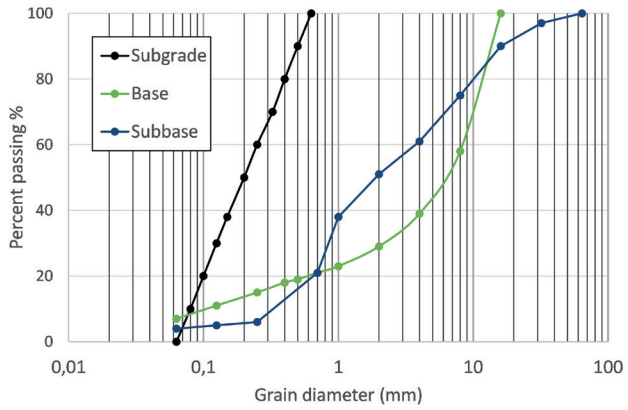

Fig. 1 Particle size distribution of the pavement layers

It was assumed based on the Hungarian Design and Specification Standard [18] that the subgrade with 93% Proctor compaction has an E_2 of approx. 35 MPa in unfavorable geohydrological conditions; this requires the construction of a subbase course. It was also assumed that the subbase course has a Proctor compaction of 95%. Bearing capacity (E_2) modulus of the subbase course material based on the back-analysis of plate load tests performed by [15] is approx. 150 MPa, thus an E_2 of 60 MPa can be expected on top of the 20-cm thick subbase course. Bearing capacity modulus of the base course material (crushed stone) based on finite element back-analysis is approx. 230 MPa, thus an E_2 of 120–125 MPa can be expected on top of the 20-cm thick base course, which corresponds to the required values presented in the literature.

3 Finite element model

In order to obtain better understanding of earth pressures and strains developing in the soil beneath pavements, geotechnical finite element modelling was performed in Plaxis [19] using the pavement structures and materials presented in Section 2. The pavement layers were modelled using the HS-Small material model except for the asphalt course, which was assumed to be linearly elastic. Since the parameters for the HS-Small material model were only partially available, the finite element model was partly calibrated with literature data, partly with the results of laboratory tests carried out on the specific materials, and partly with the "back analysis" of on-site bearing capacity measurements.

The load of construction traffic and heavy machineries, i.e., the pre-consolidation pressure was estimated to be 150 kPa in accordance with practical experience. In the first step, parameters of the sand subgrade were defined based on literature data and experience. Shear strength parameters were determined based on standard static laboratory tests presented in [14] and dilatancy angle of the material was approximated with the commonly used relationship of quartz sands: $\psi = \varphi - 30°$ [19]. The exponent "m" was chosen as 0.5, typical for granular materials [19, 20]. Small strain parameters (G_0^{ref}, $\gamma_{0.7}$) for the sand were calculated using the relationships of [14, 21, 22], from d_{50} and C_U. Then, large strain stiffness parameters (E_{50}, E_{oed}, E_{ur}) were calibrated so that the finite element model gave as a result $E_2 = 35$ MPa and approx. $E_2/E_1 = 2.5$ according to the field tests. Because there is no other layer beneath the subgrade, this bearing capacity modulus can be considered as the modulus of the material itself.

Table 2 Parameters of the modelled pavement layers

Property	Subgrade	Subbase	Crushed stone base
d_{50} (mm)	0.2	2.0	6.3
C_U (-)	3.0	11.9	100.0
e_{min} (-)	0.540	0.364	0.230
e_{max} (-)	0.920	0.513	0.440
ρ_d^{min} (g/cm^3)	1.75	2.06	2.30
Proctor compaction (%)	93	95	96
Bearing capacity modulus of the material itself E_2 (MPa)	35	150	230

In the second step, parameters of the subbase course were calibrated based on laboratory test results and using the back analysis of plate load test results on a test section presented in detail in [15]. Shear strength parameters were obtained from UU triaxial test reports, the moduli for primary loading were determined by linear curve fitting on the σ–ε diagram. The exponent "m", dilatancy angle and $\gamma_{0.7}$ were determined in the same way as for the subgrade. Then, E_{ur} and G_0 values were calibrated so that the finite element model matched with the result of the in-situ plate load tests. Based on these, bearing capacity modulus of the material of the subbase course itself is approx. 150 MPa. Shear strength and large strain stiffness parameters of the crushed stone aggregate base course were determined following the laboratory tests results presented in [16]. The exponent "m", dilatancy angle and $\gamma_{0.7}$ were obtained in the same way as for the subgrade. Then, E_{ur} and G_0 were calibrated so that the finite element model gave $E_2 = 120$ MPa on top of the base course. Parameters used in the HS-Small material model are summarized in Table 3.

The finite element model of the analyzed road section exemplary for traffic load class "C" is shown in Fig. 2 with the main geometrical and physical variables of each layer.

Table 3 HS-Small parameters of the modelled layers

Parameters	Sandy subgrade	Subbase course	Crushed stone base course
$E_{50,ref}$ (MPa)	43	37.5	65
$E_{oed,ref}$ (MPa)	43	37.5	60
$E_{ur,ref}$ (MPa)	87.5	250	325
m (-)	0.5	0.5	0.5
φ (°)	34	42	45
c (kPa)	5	9	16
ψ (°)	4	12	15
$\gamma_{0,7}$	1.5 10^{-4}	1.5 10^{-4}	1.5 10^{-4}
$G_{0,ref}$ (MPa)	95	385	450

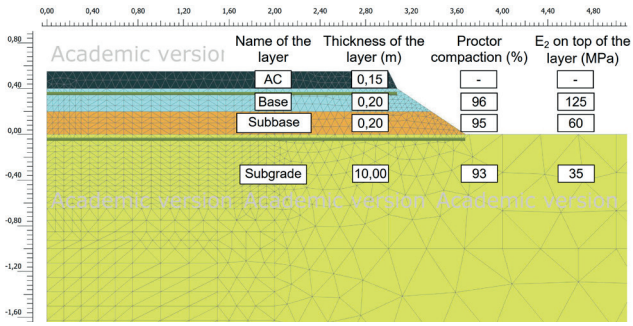

Fig. 2 Finite element model of the analyzed road section "C" with the main geometrical and physical variables

The construction sequence and the compacting effect of heavy machineries were modelled in subsequent calculation phases. The back-analysis of the on-site bearing capacity tests used for calibrating material parameters were modelled in side branches, so they didn't have any effect on the subsequent construction phases. Since one of the goals was to investigate the dependence of the stress and strain states of pavement structures on the intensity of traffic loading, the axle load was varied between 2–4–6–8–10–12 tons in the analysis. In the finite element analysis, the following construction phases were used:

1. Compaction of the formation level due to construction traffic and compaction machinery, applying their equivalent load, and quality control of the subgrade by plate load testing.
2. Construction of the subbase course, applying the equivalent construction load and quality control of the layer.
3. Construction of the crushed stone base course, applying the equivalent construction load and quality control of the layer.
4. Construction of the asphalt course and applying the equivalent construction load.
5. Standardized wheel load from the first cycle.
6. Standardized wheel load in steps of 2–4–6–8–10 tons from the second cycle.

All the horizontal strains and stresses presented hereinafter show the results from reloading.

4 Results for the coefficient of earth pressure

In the case of normally consolidated soils, the horizontal stress can be determined from the vertical stress using a strain-dependent earth pressure coefficient. When there is no horizontal deformation, the horizontal stress can be calculated using the coefficient of earth pressure at rest, K_0^{NC}. If the soil body deforms horizontally, two extreme values can be defined for the coefficient of earth pressure: K_a representing the active state when the soil loosens, and K_p representing the passive state when the soil is compressed. Gotschol [23] considers anisotropic stress state in his analysis of track ballast. It was assumed in his analysis that the soil loosens laterally in transverse direction, thus the coefficient of earth pressure used for the calculation was taken as the average of K_0 and K_a following German practice. In longitudinal direction, the coefficient of earth pressure at rest was kept as the soil cannot loosen in this direction.

If a soil was subjected to a larger overburden pressure at any point in its history than the current pressure, the soil is called overconsolidated. The coefficient of earth pressure for overconsolidated soils is larger than for normally consolidated soils. Let's take the example of one-dimensional compression test, where the soil specimen is subjected to a vertical load of $\sigma_{zz} = p$, then it is unloaded to a vertical load of $\sigma_{zz} = \sigma_{zz}^0$ (Fig. 3).

During unloading, the soil behaves nearly elastically, thus its behavior can be described by the Hooke's law (Eq. (3)). After unloading, the coefficient of earth pressure of the

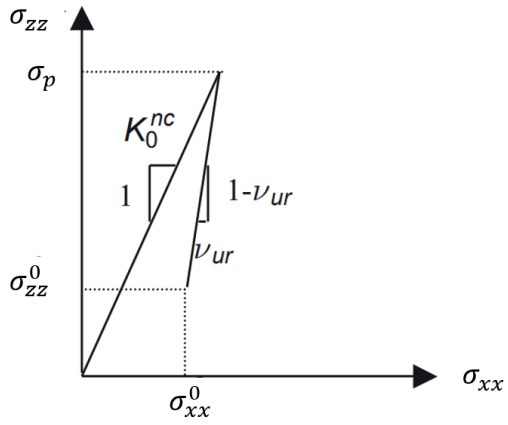

Fig. 3 Overconsolidated stress state obtained from primary loading and subsequent unloading, on the basis of [19]

overconsolidated soil in the point of σ_{zz}^{0}–σ_{xx}^{0} can be determined using Eq. (4). As it can be seen, if the unloading-reloading Poisson's ratio is small, the coefficient of earth pressure will be significantly larger than that of normally consolidated soils.

$$\frac{\Delta\sigma_{xx}}{\Delta\sigma_{zz}}=\frac{K_0^{NC}\sigma_p-\sigma_{xx}^0}{\sigma_p-\sigma_{zz}^0}=\frac{K_0^{NC}OCR\sigma_{zz}^0-\sigma_{xx}^0}{(OCR-1)\sigma_{zz}^0}=\frac{\nu_{ur}}{1-\nu_{ur}}, \quad (3)$$

$$\frac{\sigma_{xx}^0}{\sigma_{zz}^0}=K_0^{NC}OCR-\frac{\nu_{ur}}{1-\nu_{ur}}(OCR-1), \quad (4)$$

where:

σ_{xx} is the horizontal stress,
σ_{zz} is the vertical stress,
σ_p is the vertical preloading stress,
OCR is the overconsolidation ratio,
K_0^{NC} is the earth pressure coefficient at rest for normally consolidated soils,
ν_{ur} ist the unloading-reloading Poisson's ratio,
σ_{xx}^0 and σ_{zz}^0 are the horizontal and vertical stresses after unloading.

Soils beneath road pavements can be considered as overconsolidated. This is due to the significant pressure generated by compaction and the traffic of heavy machineries during construction. Because fills are generally constructed in layers of max 20–40 cm thickness, construction machines pass on top of every layer. Moreover, the construction load acts directly on top of the layer, whereas after completing the pavement, the load acting on the layers will be smaller due to stress distribution. Thus, stresses in the soil and layers of the pavement during construction are considerably larger than during operation of the road. Consequently, OCR is bigger than 1 and $K_{xy} \neq K_0^{NC}$. The goal of this research was to determine the function for $K_{xy}(z) = \sigma_x(z)/\sigma_y(z)$ in such a case. Because the value of OCR is also the function of the actual overburden pressure by definition, the value of K_{xy} is constantly changing with load steps.

The coefficient of earth pressure was analyzed with depth in all traffic load classes according to Table 1 in the finite element model presented in Section 3 with an axle load that was increased in steps of 2 tons. The coefficient of earth pressure with depth for the crushed stone aggregate base course and the subbase course for load classes of A-C-E-R is shown in Fig. 4.

Fig. 4 shows that the value of K_{xy} decreases gradually as the load increases. This is logical as the coefficient of earth pressure is proportional to the OCR according to Eq. (4).

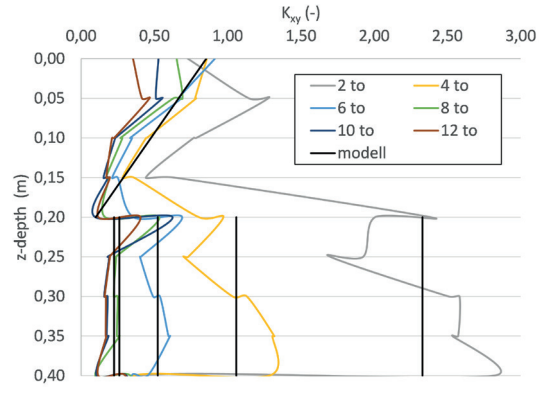

(a) Traffic load class "A"

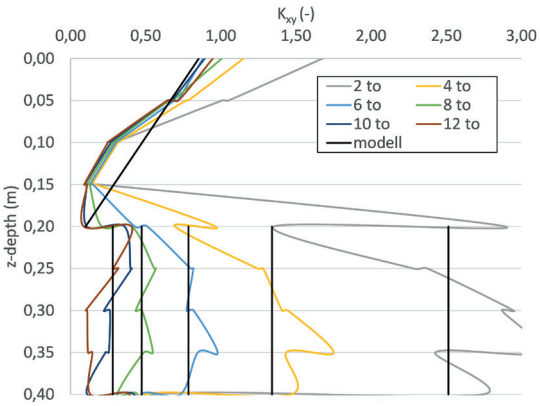

(b) Traffic load class "C"

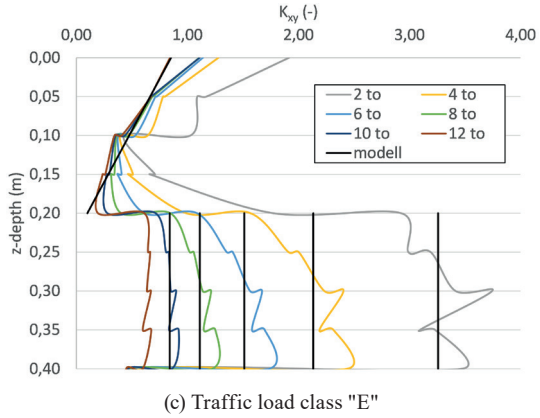

(c) Traffic load class "E"

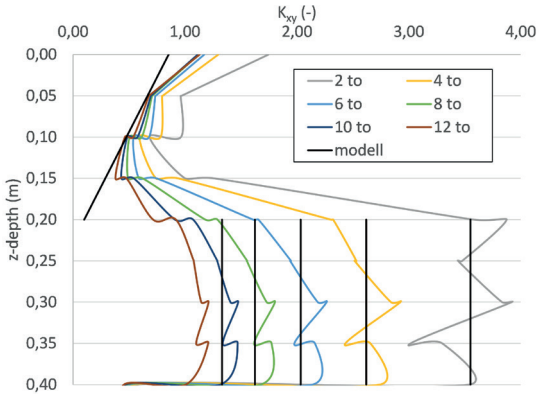

(d) Traffic load class "R"

Fig. 4 Coefficients of earth pressure in the base and subbase courses as obtained from the finite element modelling and approximation of them

Accordingly, if the load increases, the OCR will decrease, and the coefficient of earth pressure will also decrease. It can also be concluded that K_{xy} decreases linearly with depth in the base course. However, this is not entirely true at the boundary of the subbase and base courses especially in pavements of higher traffic load classes and for smaller axle loads. Nevertheless, let's accept for the sake of simplicity that the $K_{xy}(z)$ function in the base course can be approximated with a straight line regardless of the traffic load class and load level. Accordingly, Eq. (5) was fitted using the least squares method and the parameters listed in Table 4 were obtained as a result. The coefficient of earth pressure obtained in this way overestimates the actual earth pressure that was given by the finite element model in lower traffic load classes and underestimates it in higher traffic load classes, but it gives a fairly accurate result in medium traffic load classes of "C"–"D".

This means that higher horizontal stress is considered in lower traffic load classes, whereas lower horizontal stress is considered in higher traffic load classes.

$$K_{xy}^{base}(z) = K_{xy,max}^{base} - \left(z \frac{K_{xy,max}^{base} - K_{xy,min}^{base}}{d_{base}} \right), \tag{5}$$

where:

$K_{xy}^{base}(z)$ is the earth pressure coefficient function in the base course,

d_{base} is the thickness of the base course,

$K_{xy,\max}^{base}$ and $K_{xy,\min}^{base}$ are the earth pressure coefficients at the top and at the base of the crushed stone base course, respectively.

The function of $K_{xy}(z)$ in the subbase course is shown in Fig. 4. The values of K_{xy} are significantly higher than 1.0 for smaller axle loads. The reason for this is that although the subbase course is subjected to almost the same load during construction as the crushed stone base course, the actual stress during operational traffic is much lower in it than in the base course due to the stress distribution in the asphalt and base courses, thus $OCR^{sb} > OCR^{base}$, and K_{xy}^{sb} is larger than K_{xy}^{base}. On the other hand, it can also be concluded that as the load increases, the value of K_{xy} gradually decreases, which according to Eq. (4) is also logical because the value of K_{xy} will also decrease if the OCR decreases. Thirdly, it can also be seen that as the traffic load class gets higher, the K_{xy} also increases. The reason for this is that the higher the traffic load class, the thicker is the asphalt course, so the pressure acting on the subbase course from the wheel load is smaller, which increases the OCR and thus the coefficient of earth pressure as well. In the subbase course, the coefficient of earth pressure increases slightly with depth for smaller loads, while it may even decrease for higher loads in low traffic load classes. Due to the above reasons, the definition of a uniform and sufficiently accurate correlation that is valid for the entire loading process and for all traffic load classes is not possible. Therefore, the coefficient of earth pressure in the subbase course was approximated with constants independent of the depth (Table 5).

The coefficients of earth pressure in the subgrade determined using the above presented finite element model is summarized in Fig. 5 for traffic load classes A-C-E-R. It can be observed that as the load increases, the value of K_{xy} decreases in all traffic load classes (this trend is similar to the base course). Furthermore, in the upper layers by moderate axel loads the value of K_{xy} is dependent on the traffic load class. On the other hand, in the deeper layers the dependence is negligible. The shape of the $K_{xy}(z)$ function is the same regardless of the traffic load class. From the initial value of approx. $K_{xy} = K_0^{NC}$, it gradually increases to a depth of approx. 1–1.5 m below the top of the layer, and then it starts to decrease with depth.

Fig. 5 also reflects that depth of the peak value shifts towards the top of the layer as the thickness of the asphalt course (traffic load class) increases. As the shape of the function is almost the same in all traffic load classes and the values increase uniformly with the load, a single relationship

Table 4 Earth pressure coefficient at the top ($K_{xy,\max}^{base}$) and at the base ($K_{xy,\min}^{base}$) of the crushed stone base course

Coefficient of earth pressure	Independently of traffic load class
$K_{xy,\max}^{base}$	0.85
$K_{xy,\min}^{base}$	0.10

Table 5 Coefficient of earth pressure (K_{xy}^{sb}) in the subbase course in the function of traffic load class and wheel load

Traffic load class	K_{xy}^{sb} Load step (t)					
	0	2	4	6	8	10
A	6.55	2.33	1.06	0.52	0.26	0.23
B	6.14	2.66	1.19	0.63	0.32	0.19
C	6.02	2.51	1.34	0.79	0.47	0.28
D	5.90	2.95	1.74	1.11	0.74	0.50
E	5.93	3.26	2.13	1.51	1.11	0.84
K	5.11	3.43	2.41	1.79	1.38	1.08
R	5.65	3.55	2.62	2.03	1.63	1.33

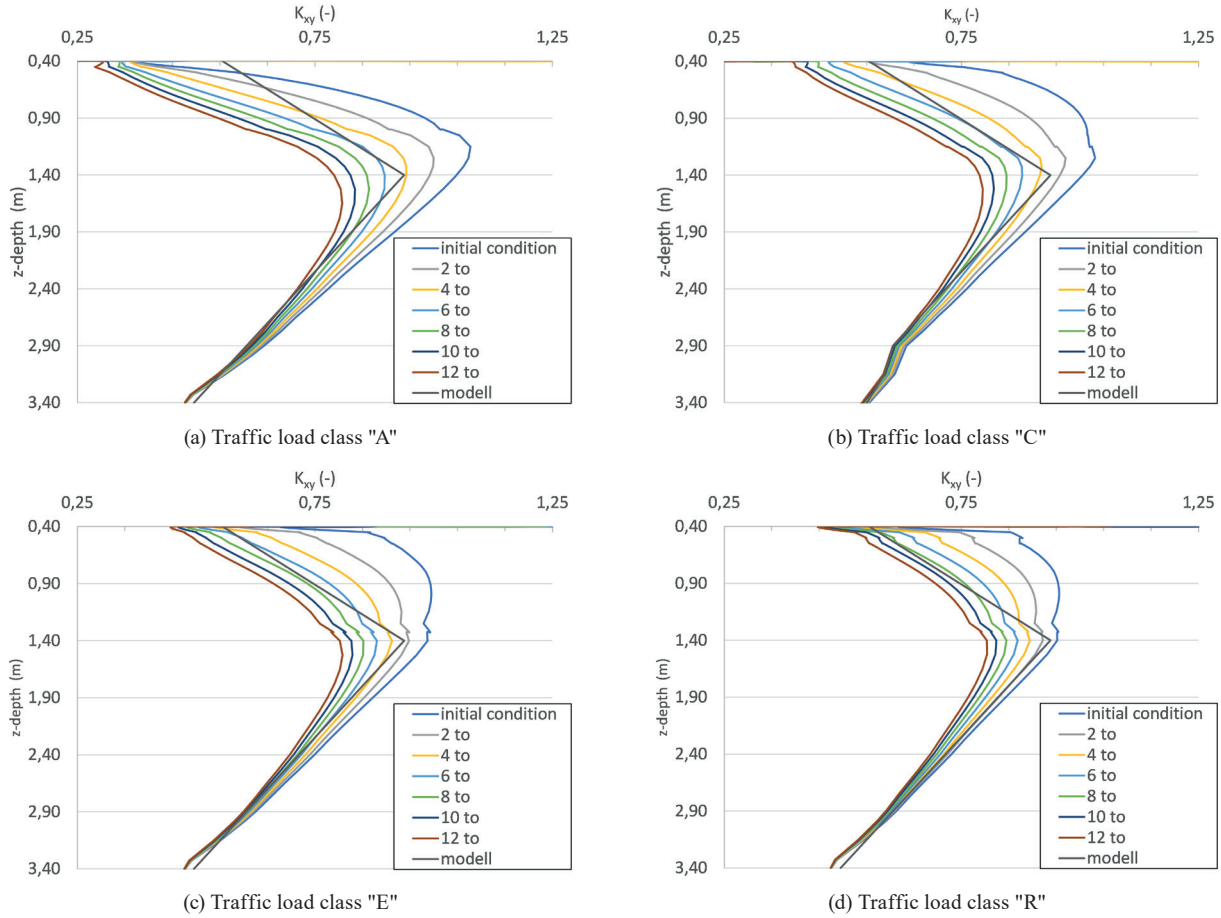

(a) Traffic load class "A"

(b) Traffic load class "C"

(c) Traffic load class "E"

(d) Traffic load class "R"

Fig. 5 Coefficients of earth pressure in the subgrade as obtained from the finite element modelling and approximation of them

can be used as an approximation to describe the horizontal stresses. This relationship was determined by fitting Eqs. (6) and Eq. (7) using the least squares method and the obtained parameters are summarized in Table 6. Due to this approximation, the coefficient of earth pressure given by the finite element model is overestimated in the upper part of the layer in lower traffic load classes ("A"–"B"), while a fairly accurate estimation is obtained in medium traffic load classes ("C"–"D"). In higher traffic load classes ("K"–"R"), the equation tends to underestimate the coefficient of earth pressure in the upper part, while it overestimates it in the middle and bottom parts of the layer.

$$K_{xy}^{sg}(z) = K_{xy,top}^{sg} - \left[\left(z - d_{base} - d_{sb} \right) \frac{K_{xy,top}^{sg} - K_{xy,max}^{sg}}{1{,}0} \right] \quad (6)$$

for $d_{base} + d_{sb} \le z \le d_{base} + d_{sb} + 1.0$,

$$K_{xy}^{sg}(z) = K_{xy,max}^{sg} - \left[\left(z - d_{base} - d_{sb} - 1 \right) \frac{K_{xy,max}^{sg} - K_{xy,bottom}^{sg}}{d_{sg} - 1} \right]$$

for $d_{base} + d_{sb} + 1.0 < z$, (7)

where:

$K_{xy}^{sg}(z)$ is the earth pressure coefficient function in the subgrade,

d_{base} and d_{sb} are the thickness of the base and subbase course,

$K_{xy,top}^{sg}, K_{xy,\max}^{sg}$, and $K_{xy,bottom}^{sg}$ are the earth pressure coefficients at the top, at the peak and at the base of the subgrade, respectively.

5 Strain state

The developing vertical strain due to $\Delta\sigma_1$ pressure can be calculated using the three-dimensional Hooke's law Eq. (8):

$$\Delta\sigma_1 = \frac{E}{(1+\upsilon)(1-2\upsilon)} \left[(1-\upsilon) \cdot \varepsilon_1 + \upsilon \cdot \varepsilon_2 + \upsilon \cdot \varepsilon_3 \right], \quad (8)$$

where E is the Young's modulus, υ is the Poisson's ratio.

Table 6 Coefficient of earth pressures in the sand subgrade

Coefficient of earth pressure	Regardless of load class
$K_{xy,top}^{sg}$	0.55
$K_{xy,\max}^{sg}$	0.94
$K_{xy,bottom}^{sg}$	0.62

Let's determine the lateral strains, ε_2 and ε_3, in the function of vertical strain by assuming that the strains in the two lateral directions are the same due to the axisymmetric condition (Eq. (9)).

$$\varepsilon_2 = \varepsilon_3 = \vartheta\varepsilon_1 , \tag{9}$$

where ϑ is the ratio of the lateral and vertical strain.

Combining Eq. (8) and Eq. (9) and rearranging to ε gives Eq. (10).

$$\Delta\varepsilon_1 = \frac{\Delta\sigma_1}{E}\frac{(1+\upsilon)(1-2\upsilon)}{1-\upsilon+2\upsilon\vartheta} \tag{10}$$

In conventional settlement calculations below footings or in the axis of large embankments, K_0 stress state is assumed, i.e., $\varepsilon_2 = \varepsilon_3 = 0$, thus $\vartheta = 0$. Replacing $\vartheta = 0$ in Eq. (10) yields the constrained modulus (E_s) and the equation becomes the well-known relationship used in conventional settlement analysis (Eq. (11)).

$$\Delta\varepsilon_1 = \frac{\Delta\sigma_1}{E}\frac{(1+\upsilon)(1-2\upsilon)}{1-\upsilon} = \frac{\Delta\sigma_1}{E_s} \tag{11}$$

If it is assumed that lateral strains can freely develop (e.g., in a triaxial cell), then $\vartheta = -\upsilon$. In this case, Eq. (10) becomes the one-dimensional Hooke's law. In K0 stress state, the soil behaves stiffer due to constrained lateral deformations therefore the settlement will be less. If lateral deformations are allowed, the behavior will be softer, and more settlement will be experienced. In more complex and real life-like boundary conditions, none of the above assumptions is valid; this particularly true for the analyzed pavement problem. The dependence of the ϑ factor on depth is discussed in [24]. In their study, hypoplastic material model was used to back-calculate the ratio of strain components in the function of depth and footing geometry for statically loaded footings. Based on the results of numerical calculations, it was found that K_0 stress state is only valid directly below the footing, and then ϑ gradually increases to the depth "z", which is almost twice of the footing width (2B) and takes a final value of ϑ_∞ and then it remains constant. However, in [24] an overconsolidation as a result of pre-loading of the soil was not considered.

Using Plaxis, calculations were run in traffic load classes "A"–"R" with a stepwise load increased by 2 tons, then the resulting horizontal ε_x and vertical ε_y strains were extracted and their ϑ ratio with depth was plotted on a diagram. Fig. 6 shows this graph for traffic load class "C". As it is reflected by the figure, the functions $\vartheta(z)$ are essentially independent of the load level, the curves are almost the same; this statement is also true for the other traffic load classes not shown on Fig. 6.

Fig. 7 presents the ratio of horizontal and vertical strains with depth in traffic load classes A-C-E-R showing that ϑ is essentially independent of the traffic load class apart from slightly differences on the boundaries of layers. Therefore, it is sufficient to use a single ϑ–z relationship for all load levels and traffic load classes. Eqs. (12)–(15) and parameters in Table 7 were determined by using the least squares method, and then the parameters were slightly rounded for the sake of simplicity.

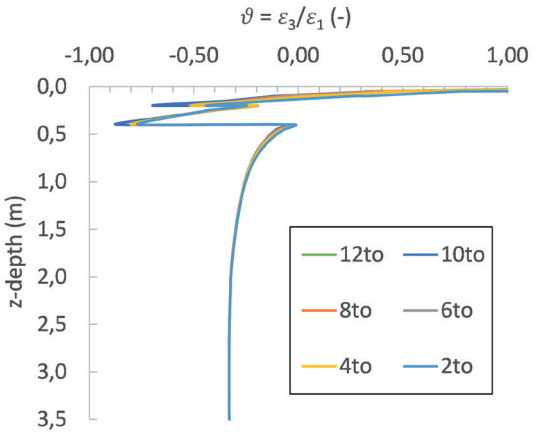

Fig. 6 Ratio of horizontal and vertical strains with depth for different loads in traffic load class "C"

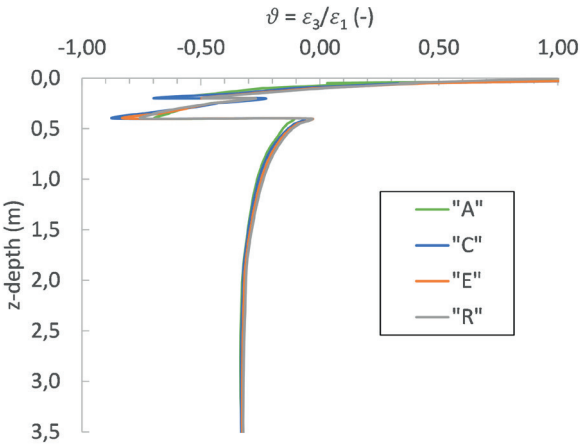

Fig. 7 Ratio of horizontal and vertical strains with depth in different traffic load classes

Table 7 Maximum and minimum values of the horizontal and vertical strain ratio

Layer	ϑ_{max}	ϑ_{min}
Crushed stone base	0.850	-0.450
Subbase	-0.300	-0.800
Sandy subgrade	-0.050	-0.325

$$\vartheta_{base}(z) = \vartheta_{max,base} + \left(z \frac{\vartheta_{max,base} - \vartheta_{min,base}}{d_{base}} \right), \quad (12)$$

$$\vartheta_{sb}(z) = \vartheta_{max,sb} + \left((z - d_{base}) \frac{\vartheta_{max,sb} - \vartheta_{min,sb}}{d_{sb}} \right), \quad (13)$$

$$\vartheta_{sg}(z) = \vartheta_{max,sb} + \left((z - d_{base} - d_{sb}) \frac{\vartheta_{max,sg} - \vartheta_{min,sg}}{0.75} \right) \quad (14)$$

for $d_{base} + d_{sb} < z \leq 0.75 + d_{sb} + d_{base}$,

$$\vartheta_{sg}(z) = \vartheta_{min,sg} \text{ for } z > 0.75 + d_{sb} + d_{base}, \quad (15)$$

where:

$\vartheta_{base}(z)$, $\vartheta_{sb}(z)$ and $\vartheta_{sg}(z)$ are the functions of the lateral and vertical strain ratio in the base, subbase, and subgrade course, respectively.

ϑ_{max} and ϑ_{min} are the fitted extreme values of the lateral and vertical strain ratio. The values in the base, subbase, and subgrade are denoted as ϑ_{base}, ϑ_{sb} and ϑ_{sg}, respectively.

d_{base}, d_{sb} are the thickness of the base and subbase course.

Fig. 8 shows the calculated and fitted curves with depth in the base and subbase courses. Note that is almost linear in the crushed stone base course and its value can even be positive at the top of the layer, while it is smaller than the value of the Poisson's ratio at the bottom. The positive ϑ is somewhat surprising, since it means that the soil compresses in both vertical and horizontal directions, which is an unusual behavior for soils. The point where no horizontal deformation occurs is at the middle of the layer. This unusual observation can be explained by the behavior of the crushed stone as it behaves like a beam under the wheel load and is bent around its neutral axis located approximately in its center line (similar behavior as in the asphalt course). As a result of this bending, compression occurs horizontally in the upper part of the layer, while the "tension" at the bottom of the layer decreases the horizontal stress, which in turn further increases the horizontal strains.

In the subgrade, the ratio of horizontal and vertical strains was similar to that of presented in the literature of footings without preloading [24]. Accordingly, the top of the subgrade can be characterized by K_0 stress state where horizontal deformations are basically zero, and then the strain ratio decreases gradually to $\vartheta_{max} \sim -\upsilon$ where the horizontal strains are unconfined. This is represented on Fig. 9.

6 Conclusions

When designing pavements, the stiffness and resilient behavior of the soil are among the most important input data. Since the stiffness of granular soils is highly influenced by the mean effective normal stress, its determination is of particular importance. In pavements, horizontal stresses generally differ from those of conventional soils because of the preloading of the pavement during construction.

In this research, finite element program and advanced material models were used to investigate the horizontal and vertical stresses and strains developing in standardized pavement cross-sections defined in accordance with [1]. Preloading resulting from the construction and compaction of the different pavement layers was taken into account. Since pavements are generally built in layers, machines used for the construction pass on top of each layer. In addition, construction loads act directly on the top of each layer, while after the pavement is completed, smaller loads will act on them due to stress distribution. Thus, stresses acting on the layers during construction are much higher than stresses acting on them during operation of the road. Consequently, OCR is higher than 1 and thus $K_{xy} \neq K_0^{NC}$. One of the main goals of this research was to investigate

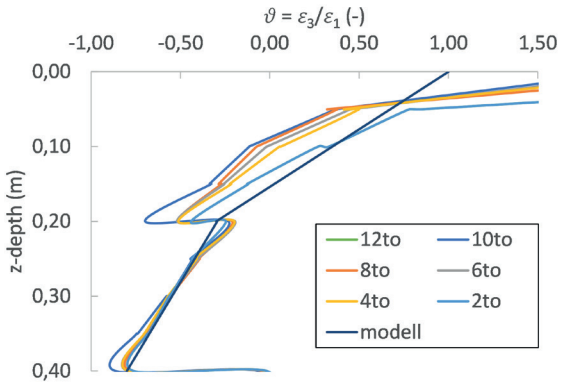

Fig. 8 The calculated and fitted ϑ functions with depth in the base and subbase courses in traffic load class "C"

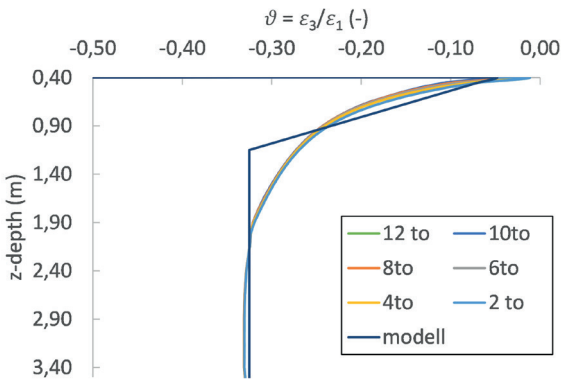

Fig. 9 The calculated and fitted ϑ functions with depth in the subgrade in traffic load class "C"

how vehicles with different axle loads affect the stress and strain state of pavement structures, thus the axle load in the analysis was varied between 2–4–6–8–10–12 tons.

The coefficient of earth pressure in pavements was analyzed with depth in all traffic loading classes using the finite element model presented above with an axle load that was increased in steps of 2 tons. The coefficient of earth pressure gradually increases as the load increases. This is logical as the coefficient of earth pressure is proportional to the OCR. Accordingly, if the load increases, the OCR will decrease, and the coefficient of earth pressure will also decrease. It is also concluded that K_{xy} decreases linearly with depth in the crushed stone base course. A recommendation was presented in Eq. (5) and Table 4 with which the $K_{xy}(z)$ function can be approximated independently of the load and the traffic load class.

In the subbase course, the value of K_{xy} is significantly higher than 1.0 especially lower axle loads. The reason for this is that although the subbase course is subjected to almost the same load during construction as the crushed stone base course, the actual stress during operational traffic is much lower in it than in the crushed stone due to the stress distribution in the asphalt and the crushed stone layers, thus $OCR^{sb} > OCR^{base}$, and K_{xy}^{sub} is larger than K_{xy}^{base}. In the subbase course, the coefficient of earth pressure increases slightly with depth for lower loads, while it may even decrease for higher loads in low traffic load classes. Due to the above reasons, the definition of a uniform and sufficiently accurate correlation that is valid for the entire loading process and for all traffic load classes is not possible. Therefore, the coefficient of earth pressure in the subbase course was approximated with constants independent of the depth (Table 5).

Shape of the $K_{xy}(z)$ function in the subgrade is the same regardless of the traffic load class. From the initial value of approx. $K_{xy} = K_0^{NC}$, it gradually increases to the depth of approx. 1–1.5 m below the top of the layer, and then it starts to decrease with depth. Depth of the peak value shifts towards the top of the layer as thickness of the asphalt course (traffic load class) increases. As the shape of the function is almost the same in all traffic load classes and the values increase uniformly with the load, a single relationship can be used as an approximation to describe the horizontal stresses. This relationship was determined by fitting Eq. (6) and Eq. (7) using the least squares method and the obtained parameters are summarized in Table 6.

Using Plaxis, calculations were run in traffic load classes A-R with a stepwise load increased by 2 tons, then the resulting horizontal ε_x and vertical ε_y strains were extracted and their ϑ ratio with depth was plotted on a diagram. The function $\vartheta(z)$ is essentially independent of the load intensity and the traffic load class. The $\vartheta(z)$ is almost linear in the crushed stone base course and its value can even be positive at the top of the layer, which can be explained by the plate-like behavior of the crushed stone aggregate. On the other hand, the ratio of horizontal and vertical strains in the subgrade was similar to that of presented in the literature of footings. Accordingly, the top of the subgrade can be characterized by K_0 stress state where horizontal deformations are basically zero, and then the strain ratio decreases gradually with depth to $\vartheta_{max} \sim -\upsilon$ where the horizontal strains are unconfined. Recommendation (Eqs. (12)–(15) with the parameters presented in Table 7) was given to approximate the function of the ratio of horizontal and vertical strains with depth.

References

[1] Hungarian Road Association "e-UT06.03.13 Aszfaltburkolatú útpályaszerkezetek méretezése és megerősítése" (Design of Road Pavement Structures and Overlay Design with Asphalt Surfacing), Road Design and Specification Standard, Hungary, 2005. [online] Available at: https://ume.kozut.hu/dokumentum/193 (in Hungarian)

[2] Forschungsgesellschaft für Straßen- und Verkehrswesen "RStO, Richtlinie für die Standardisierung des Oberbaues von Verkehrsflächen" (Guidelines for the standardisation of pavement structures of traffic areas), Germany, 2001. (in German)

[3] AASHTO "AASHTO Guide for Design of Pavement Structures 1993", American Association of State Highway and Transportation Officials, Washington, DC, USA, 1993.

[4] Brown, S. F., Brunton, J. M., Stock, A. F. "The analytical design of bituminous pavements", Proceedings of the Institution of Civil Engineers, 79(1), pp. 1–31, 1985. https://doi.org/10.1680/iicep.1985.1077

[5] Freeme, C. R., Maree, J. H., Vilojen, A. W. "Mechanistic design for asphalt pavements and verification using the Heavy Vehicle Simulator", In: Proceedings of 5th International Conference on the Structural Design of Asphalt Pavements, Delft, Netherlands, 1982, pp. 156–173.

[6] Shell "SHELL SPDM-PC User manual: Shell pavement design method for use in a personal computer", Version 1994, Release 2.0, Shell International Petroleum, London, UK, 1994.

[7] Hardin, B. O., Black, W. L. "Sand Stiffness Under Various Triaxial Stresses", Journal of the Soil Mechanics and Foundations Division, 92(2), pp. 27–42, 1966. https://doi.org/10.1061/JSFEAQ.0000865

[8] Ishibashi, I. "Discussion of Effect of Soil Plasticity on Cyclic Response", Journal of Geotechnical Engineering, 118(5), pp. 830–832, 1992. https://doi.org/10.1061/(ASCE)0733-9410(1992)118:5(830.2)

[9] Shaw, P. S. "Stress-Strain Relationships for Granular Materials under Repeated Loading", PhD Thesis, University of Nottingham, 1980.

[10] Lekarp, F., Isacsson, U., Dawson, A. "State of the Art. I: Resilient Response of Unbound Aggregates", Journal of Transportation Engineering, 126(1), pp. 66–75, 2000. https://doi.org/10.1061/(ASCE)0733-947X(2000)126:1(66)

[11] Häcker, A. "Erweiterung eines Lamellenmodells für zyklisch belastete Flachgründungen" (Extension of a Laminal Modell for Cyclic Loaded Foundations), Karlsruher Institute für Technologie, Institute für Bodenmechanik und Felsmechanik, Karlsruhe, Germany, 2013. (in German)

[12] Wöhrle, T. "Überprüfung und Entwicklung einfacher Ingenieurmodelle für Offshore-Windenerigealagen auf Bass eines Akkumulationsmodells" (Examination and Development of Simplified Engineering Oriented Model for Offshore Wind Turbins on the Basis of an Accumulation Modell), Graduation Thesis, Karlsruher Institute für Technologie, Institute für Bodenmechanik und Felsmechanik, 2012. (in German)

[13] Zachert, H. "Zur Gebrauchstauglichkeit von Gründungen für Offshore-Windenergieanlagen" (On the Usability of Foundations for Offshore Wind Turbins), PhD Thesis, Karlsruher Institut für Technologie (KIT), 2015. (in German)

[14] Wichtmann, T. "Soil behaviour under cyclic loading - experimental observations, constitutive description and applications", Habilitation Thesis, Karlsruher Institut für Technologie (KIT), 2016.

[15] Káli, A. "Ipari padlók ágyazatként és útépítési védőrétegként használt durvaszemcsés talaj sajátmodulusának numerikus modellezése" (Numerical Analysis of the Bearing Capacity Modulus of Course Soils Used in Pavement and Industrial Slab Layers), BSc Thesis, Budapest University of Technology and Economics, 2020. (in Hungarian)

[16] Rondón, H. A., Wichtmann, T., Triantafyllidis, T., Lizcano, A. "Hypoplastic material constants for a well-graded granular material for base and subbase layers of flexible pavements", Acta Geotechnica, 2, pp. 113–126, 2007, https://doi.org/10.1007/s11440-007-0030-3

[17] Wichtmann, T., Rondón, H., Niemunis, A., Triantafyllidis, T., Lizcano, A. "Prediction of Permanent Deformations in Pavements Using a High-Cycle Accumulation Model", Journal of Geotechnical and Geoenvironmental Engineering, 136(5), pp. 728–740, 2010. https://doi.org/10.1061/(ASCE)GT.1943-5606.0000275

[18] General Department of Economics and Road Transportation "ÚT 2-1.222, Utak és autópályák létesítésének általános geotechnikai szabályai" (General geotechnical Specifications for te Establisment of Roads and Highways), Budapest, Hungary, 2006. (in Hungarian)

[19] Plaxis "Plaxis Material Models Manual", Version 8, 2011.

[20] Janbu, N. "Soil models in offshore engineering", Géotechnique, 35(3), pp. 241–281, 1985. https://doi.org/10.1680/geot.1985.35.3.241

[21] Wichtmann, T., Triantafyllidis, T. "Effect of Uniformity Coefficient on G/Gmax and Damping Ratio of Uniform to Well-Graded Quartz Sands", Journal of Geotechnical and Geoenvironmental Engineering, 139(1), pp. 59–72, 2013. https://doi.org/10.1061/(ASCE)GT.1943-5606.0000735

[22] Wichtmann, T., Triantafyllidis, T. "Influence of the Grain-Size Distribution Curve of Quartz Sand on the Small Strain Shear Modulus Gmax", Journal of Geotechnical and Geoenvironmental Engineering, 135(10), pp. 1404–1418, 2009. https://doi.org/10.1061/(ASCE)GT.1943-5606.0000096

[23] Gotschol, A. "Veränderlich elastisches und plastisches Verhalten nichtbindiger Böden und Schotter unter zyklisch-dynamischer Beanspruchung" (Varying Elastic an Plastic Behaviour of Non-Cohesive Soils and Gravels Under Cylclic-Dynamic Strains), University of Kassel, Department of Geotechnics, Kassel, Germany, 2002. (in German)

[24] Nübel, K., Karcher, C., Herle, I. "Ein einfaches Konzept zur Abschätzung von Setzungen" (A Simplified Concept to Estimate Settlements), Geotechnik, 4(22), pp. 251–258, 1999. (in German)